Inner-Phase Reaction Dynamics: The Influence of Hemicarcerand Polarizability and Shape on the Potential Energy Surface of an Inner-Phase Reaction

Sigifredo Sánchez Carrera,[a] Jean-Luc Kerdelhué,[b] Kevin J. Langenwalter,[b] Neil Brown,[b] and Ralf Warmuth*[b,c]

Keywords: Polarizability / Hemicarcerand / Host–guest systems / Encapsulation / Solvent effect / Diazirines

The thermal decomposition of six phenyldiazirine (**2**) hemicarceplexes and the spectroscopic properties of these hemicarceplexes, as well as those of one spiro[cyclobutabenzene-1(2*H*),3′-diazirine] (**1**) and one *p*-tolyldiazirine (**3**) hemicarceplex, have been investigated in order to determine the effect of a hemicarcerand on the potential energy surface of an inner-phase reaction. These hemicarceplexes have pentyl or phenethyl feet groups, three tetramethylene linkers and differ in the nature of one linker group X as follows: **1**: X = $(CH_2)_5$; **2**: X = $(CH_2)_n$ (n = 2, 3, 4), (*S,S*)-$CH_2CH[OC(CH_3)O]CHCH_2$ and *ortho*-$CH_2C_6H_4CH_2$; **3**: X = $(CH_2)_4$. The effect of the linker group X on the structure of the phenyldiazirine hemicarceplexes was analyzed by MM2 force field calculations and leads to a change in the bending of the inner phase, which increases in the order (*S,S*)-$CH_2CH[OC(CH_3)O]CHCH_2$ > $(CH_2)_4$ > $(CH_2)_3$ > $(CH_2)_2$ > *ortho*-$CH_2C_6H_4CH_2$ and to a shortening of the center-to-center distance between the two cavitands of the host, which decreases in the order (*S,S*)-$CH_2CH[OC(CH_3)O]CHCH_2$ < $(CH_2)_4$ < $(CH_2)_3$ < $(CH_2)_2$ < *ortho*-$CH_2C_6H_4CH_2$. All hemicarceplexes show large red shifts of the diazirine n-π*-transition in their UV/Vis absorption spectra. From the red shifts and from plots of the n-π*-excitation energy of the free diazirines against the solvent polarizability *P*, the inner-phase polarizability was estimated. *P* ranges from 0.39 to 0.58 and is larger than the polarizabilities of common organic solvents. A comparison of the activation parameters $\Delta H^{\ddagger}$, $T\Delta S^{\ddagger}$, and $\Delta G^{\ddagger}$ for the diazirine decomposition in the inner phase with those in the bulk phase shows that the hemicarcerand stabilizes the inner-phase transition states enthalpically by $\Delta\Delta H^{\ddagger}$ = 1.9–2.8 kcal/mol and destabilizes the transition states entropically by $\Delta T\Delta S^{\ddagger}$ = 0.2 to 3.0 kcal/mol. The enthalpic stabilization is explained with dispersion interactions between the stretched C–N bonds in the transition state and the highly electron-rich aryl units of the hemicarcerand. This is consistent with the high polarizability of the inner phase. The entropic destabilization of the inner-phase transition states is explained with a greater loss of vibrational degrees of freedoms as the transition state is reached in the inner phase as compared to the more mobile bulk solvent cage. Furthermore, the entropic destabilization decreases with an increased bending of the inner phase. This is explained with an induced-fit model. An increased hemicarcerand bending leads to an improved fit between the inner phase and the bend transition states, which reduces the loss of vibrational degrees of freedom as the transition states are reached.

Introduction

The investigation of reactions in the inner phase of carcerands, hemicarcerands and self-assembled capsules is of great importance to chemistry and biology and has received much attention in the past years.[1–7] Through the photochemical manipulation of incarcerated reactants, highly reactive intermediates have been generated and stabilized by preventing their dimerization or the reaction with bulk-phase reactants that are too large to enter the inner phase.[6–17] Encapsulation has also been applied to investigate fundamental aspects of electron and energy transfer processes,[18–22] to change and control the rate and regiochemistry of bimolecular reactions,[23–33] to amplify reactions,[34] and to alter the position of chemical equilibria.[35]

Recently, Rebek and co-workers and Fujita and co-workers showed that Diels–Alder reactions and photochemical [2+2] additions are strongly accelerated in the presence of a self-assembled capsule or coordination cage.[26–30] The rate-accelerating effect of the container was explained by the increased apparent reactant concentrations in the inner space. Whether part of this observed rate acceleration is due to a selective stabilization of the transition states is difficult to evaluate. Here, we address this very fun-

[a] Departamento de Química, Instituto Tecnológico y de Estudios Superiores de Monterrey,
Monterrey, N. L. 64849, México
[b] Department of Chemistry, Kansas State University,
Manhattan, Kansas 66506-3701, USA
[c] Department of Chemistry and Chemical Biology, Rutgers, The State University of New Jersey,
Piscataway, NJ 08854-8087, USA
Fax: +01-732-445-8432
E-mail: warmuth@rutchem.rutgers.edu
Supporting information for this article is available on the WWW under http://www.eurjoc.com or from the author.

 DOI: 10.1002/ejoc.200400578

damental aspect of inner-phase chemistry: What is the nature of the interaction between an inner-phase transition state and the surrounding hemicarcerand? We believe that the insight gained from addressing this question will be important for the design of novel molecular container-based catalysts and for the understanding of transition-state stabilization in enzyme-catalyzed reactions.[36–38] For this purpose, unimolecular thermal reactions are better suited as compared to bimolecular reactions. Recently, we chose the thermal decomposition of diazirines as model reaction.[39] An important consideration for choosing this reaction has been the magnitude of its activation barrier $\Delta G^{\ddagger}$ = 27 ± 3 kcal/mol.[40–43] Thus, diazirines are long-lived enough at ambient temperature to allow preparation and isolation of the corresponding hemicarceplexes. At elevated temperature the guest will likely decompose faster than the hemicarceplex dissociates. The latter requires overcoming constrictive plus intrinsic binding energy, which is generally higher.[1,44] Furthermore, the fragmentation mechanism is well established based on the experimental work by Liu and co-workers and several computational studies.[40–43,45–48] Diazirines fragment to carbenes and nitrogen or weakly bound carbene-nitrogen complexes, which either collapse to diazo compounds or yield carbene reaction products. In some cases, the direct isomerization of diazirines to diazomethanes has been observed.[48,49] We measured a large rate acceleration for the thermal decomposition of diazirine **1** upon encapsulation inside hemicarcerand **4445** and explained this rate acceleration with a transition-state stabilization through dispersion forces.[39] Contrary to **1**, the decomposition rate of phenyldiazirine (**2**) was essentially not affected or, in the case of tolyldiazirine **3**, decreased upon incarceration inside hemicarcerand **4444Phe**. In order to get more insight into the effect of the surrounding hemicarcerand on the potential energy surface of aryldiazirine decompositions, we have extended our investigation to several other phenyldiazirine hemicarceplexes, in which the shape of the host is slightly altered through variation of one linker. Our results show that all transition states are enthalpically stabilized by approximately 2.5 kcal/mol and that the modulation of the reaction rates depends on the shape complementarity between the inner phase and the transition state.

Results and Discussion

Synthesis of Hemicarceplexes: We prepared hemicarceplexes **4444Phe⊙2**,[50] **4444Pen⊙2**,[15] **4444Phe⊙3**,[39] **4444S⊙2**,[15] and **4445⊙1**[39] as described earlier. Hemicarceplexes **4442⊙2**, **4443⊙2**, and **444*o*X⊙2** were synthesized according to a general "guest-seal-in" procedure, in which

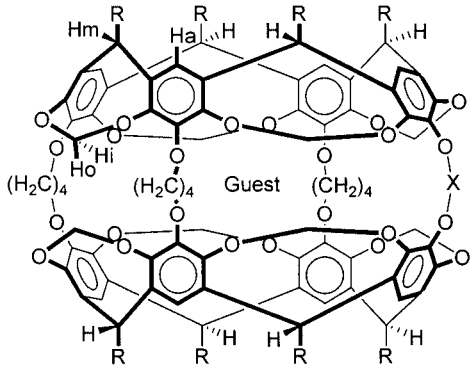

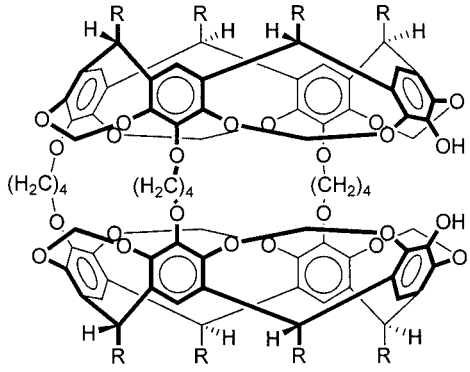

4 R = $CH_2CH_2C_6H_5$

4442⊙Guest: X = $(CH_2)_2$; R = $CH_2CH_2C_6H_5$
4443⊙Guest: X = $(CH_2)_3$; R = $CH_2CH_2C_6H_5$
4444Phe⊙Guest: X = $(CH_2)_4$; R = $CH_2CH_2C_6H_5$
4444Pen⊙Guest: X = $(CH_2)_4$; R = $CH_2(CH_2)_3CH_3$
4445⊙Guest: X = $(CH_2)_5$; R = $CH_2CH_2C_6H_5$

4444S⊙Guest X = 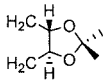 R = $CH_2(CH_2)_3CH_3$

444oX⊙Guest X =  R = $CH_2CH_2C_6H_5$

444An⊙Guest X = 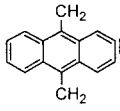 R = $CH_2CH_2C_6H_5$

Guests:

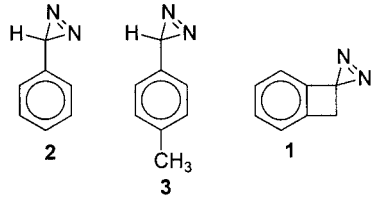

2 **3** **1**

TsO-$(CH_2)_n$-OTs

5: *n* = 2
6: *n* = 3

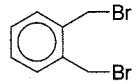

7

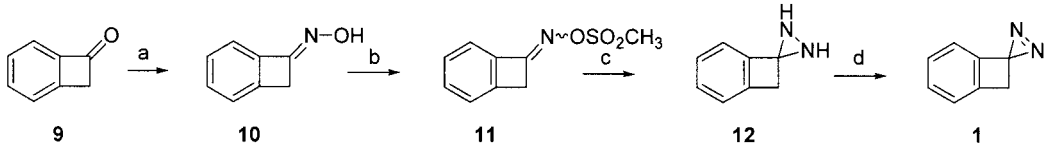

Scheme 1. Synthesis of **1**.[55] Conditions: a) NH_3OHCl; $NaHCO_3$; H_2O; 90% yield. b) MsCl; NEt_3; CH_2Cl_2; 0 °C; 85% yield. c) NH_3; ether; –25 °C; 3 d; d) $(CH_3)_3COCl$; ether; 0 °C; 50% yield over 2 steps.

the diol host **4**[51] is reacted with 4–8 equivalents of linker **5**, **6** or **7**, respectively, and Cs_2CO_3 in HMPA in the presence of excess **2**.[52,53] Yields ranged from 32% to 45% and were very sensitive to the presence of trace amounts of hydrocarbon impurities (mainly pentanes and hexanes), which were not fully removed after the column chromatographic purification of the guest.

Attempts to synthesize hemicarceplex **4445⊙1** according to our general seal-in procedure failed. Instead, we only observed products of the innermolecular reaction of carbene **8** with the surrounding host in the ^{1}H NMR spectrum of the crude reaction mixture.[54] Two of these products were isolated and characterized. For the same reason, incarceration of **1** inside **4444Phe** failed. Good yields of **4445⊙1** (80%) were obtained when we stirred empty **4445**[51] at 0 °C in $CDCl_2CDCl_2$/**1** (5:1). Guest **1** was prepared from cyclobutabenzene-1(2*H*)-one (**9**) as outlined in Scheme 1.[55] After dissolving crude **4445⊙1** in fresh $CDCl_2CDCl_2$, hemicarceplex dissociation was slow enough at elevated temperature to study the dynamics of the thermal inner-phase guest decomposition.

Thermal Inner-phase Diazirine Decomposition: Earlier, we measured the rate constants of the inner-phase guest decomposition of hemicarceplexes **4444Phe⊙2**, **4444Phe⊙3** and **4445⊙1** and compared them with those of the free guests in the same solvent.[39] Whereas **3** was thermally more stable in the inner phase of **4444Phe**, the decomposition of **2** was essentially unaffected by incarceration and that of **1** was 15-fold accelerated at 40 °C. The latter rate acceleration is remarkable since it is roughly 10-fold larger than the variation of bulk-phase decomposition rate constants of free **1** (18 different solvents; see Table S9 in supporting information, for supporting information see also the footnote on the first page of this article) and points towards a special effect of the hemicarcerand. Here, we have extended our kinetic studies to additional phenyldiazirine hemicarceplexes **4444Pen⊙2**, **4444S⊙2**, **4442⊙2**, **4443⊙2**, and **444*o*X⊙2**, in which one of the four hemicarcerand linker groups is varied. Molecular mechanical calculations (MacroModel® 7.0,[56] MM2 force field,[57] GB/SA chloroform solvation model[58]) show that this leads to a small perturbation of the inner-phase shape.[59] We tried to cap-

Table 1. UV/Vis absorption properties (λ_{max}; ε) relative local polarizability *P*, and structural features of **4445⊙1**, **4442⊙2**, **444*o*X⊙2**, **4443⊙2**, **4444Phe⊙2**, **4444Pen⊙2**, **4444S⊙2**, and **4444Phe⊙3**.

Hemicarceplex	λ_{max1} [ε]	λ_{max2} [ε]	*P*	α[a] [°]	*d*[a] [Å]	β[a] [°]
4445⊙1[b]	388.1(500)	369.0(480)	0.55	8	4.08	8.2
4445⊙1[c]	389.1(530)	369.3(520)	0.58	8	4.08	8.2
4442⊙2[c]	385.5(550)	366.3(630)	0.39	6.4	3.36	7.9
444*o*X⊙2[c]	387.1(520)	367.3(670)	0.44	8.7	3.32	11.54
4443⊙2[c]	387.2(650)	367.5(750)	0.44	4.4	3.43	8.4
4444Phe⊙2[c]	388.0(490)	367.7(550)	0.47	1.8	3.73	9.9
4444Pen⊙2[c]	387.8(580)	367.6(660)	0.47	1.8	3.73	9.9
4444S⊙2[c]	387.3(500)	367.3(560)	0.45	1.9	3.71	10.1
4444Phe⊙3[b]	396.9(660)	377.4(760)	0.52	0.8	3.95	8.0

[a] For a definition of distance *d*, tilt α and twist β, see Scheme 2. [b] In tetrachloroethane. [c] In toluene.

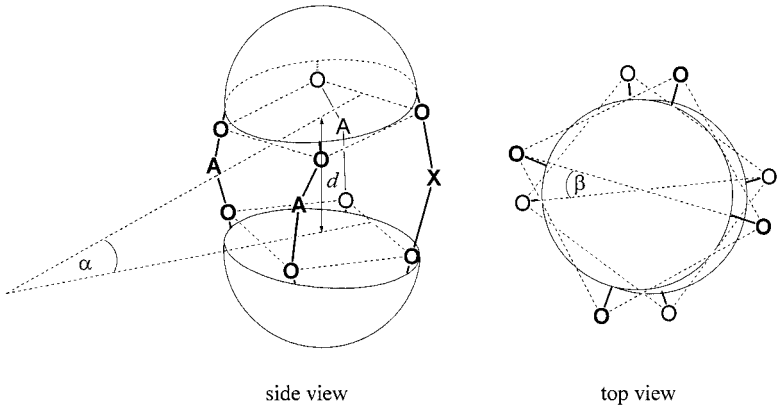

Scheme 2. Definition of center-to-center distance *d*, tilt α and twist β of the polar caps of a hemicarcerand. A = $(CH_2)_4$; X variable bridge.

ture these small changes by calculating the center-to-center distance d, the tilt α, and the relative twist β between the two planes formed by connecting the four ether oxygen atoms of each cavitand (Table 1 and Scheme 2). Based on these parameters, the structural perturbation induced by bridge X can be described as follows:[60] (1) Compared to the parent hemicarceplex **4444⊙2** with X = $(CH_2)_4$, shortening or elongating X increases α and decreases β. (2) Among the phenyl diazirine hemicarceplexes, the decrease of α correlates with a decrease of d in the order d(**4444**) ≈ d(**4444S**) > d(**4443**) > d(**4442**) > d(**444*o*X**) and α(**4444**) < α(**4444S**) < α(**4443**) < α(**4442**) < α(**444*o*X**). (3) The change of a tetramethylene (**4444**) to a 2,2-dimethyl-1,3-dioxolane-4,5-dimethylene bridge (**4444S**) has little effect on the inner-phase shape and size. (4) Elongation of the guest untwists and elongates the host.

Rate constants for the thermal decomposition of these hemicarceplexes, of **4444Phe⊙2**, and for comparison of free **2** in toluene as common bulk solvent were measured in the temperature range between approximately 60–100 °C. For hemicarceplexes **4444Phe⊙2**, **4444Pen⊙2**, **4442⊙2**, **4443⊙2** and **444*o*X⊙2**, we followed the guest decomposition by monitoring the absorbance of the diazirine chromophore above 300 nm with UV/Vis spectroscopy. Partially formed encapsulated phenyldiazomethane **13** was trapped with trifluoroacetic acid (TFA). As control experiment, we briefly photolyzed **4444Phe⊙2** in toluene containing 1% TFA and followed the dark reaction of **4444Phe⊙13** with TFA by monitoring the intensity of the diazomethane stretch at $\tilde{\nu}_{CNN}$ = 2062.2 cm^{-1}. This experiment showed that the room temperature pseudo-first order through-shell quenching rate constant k = 0.002 s^{-1} is four orders of magnitude larger than the rate constant for the inner-phase diazirine decomposition of **4444Phe⊙2**.

Representative UV/Vis spectra of **4444Phe⊙2** in toluene/1% TFA at 83.5 °C are shown in Figure 1. From the exponential decay of the absorption at 367 nm and 387 nm with time, we determined the first-order decomposition rate constant.

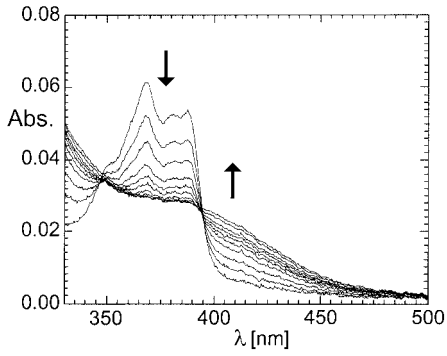

Figure 1. UV/Vis absorption spectra of **4444Pen⊙2** (1.15 μmol/ L) in toluene containing 1% (v/v) TFA at 83.5 °C at different times: t [min] = 0, 14, 28, 47, 61, 74, 90, 106, 137 and 162.

This approach failed for hemicarceplex **4444S⊙2**, for which the acid-catalyzed hydrolysis of the acetonide groups was faster than phenyldiazirine decomposition. For this hemicarceplex, we used ^{1}H NMR spectroscopy to monitor the thermal decomposition of the guest.

From the temperature dependence of the decomposition rate constants k_{IP}, we constructed Arrhenius plots (Figure 2). They provided activation energies E_a and preexponential factors A, from which we calculated the activation parameters $\Delta H^{\ddagger}_{358K}$, $T\Delta S^{\ddagger}_{358K}$, and $\Delta G^{\ddagger}_{358K}$ at 358 K. Table 2 summarizes these data together with those obtained for **4444Phe⊙3**, **4445⊙1** and **1**–**3**, $\Delta\Delta H^{\ddagger}$, $\Delta T\Delta S^{\ddagger}$ and $\Delta\Delta G^{\ddagger}$ values and inner phase to bulk-phase rate constant ratio k_{IP}/k_{BP}.

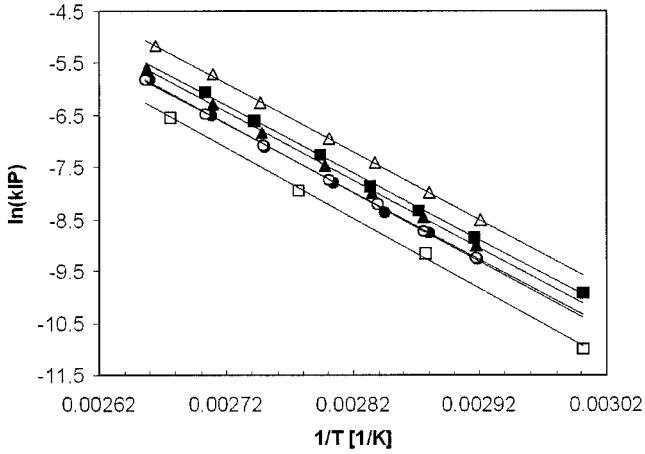

Figure 2. Arrhenius plots [ln(k_{IP}) vs. 1/T] for the thermal decomposition of hemicarceplexes **4442⊙2** (Δ), **444*o*X⊙2** (closed square), **4443⊙2** (closed triangle), **4444Phe⊙2** (open circle), **4444Pen⊙2** (closed circle) and **4444S⊙2** (open square).

We note the following interesting points and trends. (1) Among the different phenyldiazirine hemicarceplexes, k_{IP} increases in the order: **4442** > **444*o*X** > **4444Phe** = **4444Pen** > **4444S** and varies overall by a factor of 3.2. (2) All inner-phase transition states (TS) are stabilized enthalpically and are destabilized entropically as compared to the bulk-phase TS. (3) The enthalpic TS stabilization $\Delta\Delta H^{\ddagger}$ varies little among all studied hemicarceplexes: 1.9 kcal/mol ≤ $\Delta\Delta H^{\ddagger}$ ≤ 2.8 kcal/mol. (4) The variation in the entropic TS destabilization $\Delta T\Delta S^{\ddagger}$ is approximately threefold larger than that of $\Delta\Delta H^{\ddagger}$: –3.0 kcal/mol ≤ $\Delta T\Delta S^{\ddagger}$ ≤ –0.2 kcal/mol. (5) The modulation of the ratio k_{IP}/k_{BP}, which varies by a factor of 36 among all hemicarceplexes, is mainly entropic in its origin. (5) Shortening one bridge of the parent **4444Phe** by one or two methylene groups *accelerates* the decomposition contrary to our initial prediction!

We explain the common enthalpic TS stabilization of $\Delta\Delta H^{\ddagger}$ = 2.4 ± 0.5 kcal/mol with the high polarizability of the inner phase. Since the stretched C–N bonds of the transition state are more polarizable than those of the ground state, the transition state will be stronger stabilized through dispersion interactions.[61–65] The importance of polarizability in supramolecular catalysis was first pointed out by Dougherty and co-workers.[63–65] They showed that transition states of alkylation and dealkylation reactions are stabilized by 1–3 kcal/mol through dispersion forces if bond forming and breaking took place in the center of cy-

Table 2. Activation parameters (E_a, ln$A$, $\Delta G^{\ddagger}$) for the thermal decomposition of **1**–**3**, **4445⊙1**, **4442⊙2**, **444*o*X⊙2**, **4443⊙2**, **4444Phe⊙2**, **4444Pen⊙2**, **4444S⊙2**, and **4444Phe⊙3** and inner phase to bulk-phase rate-constant ratio k_{IP}/k_{BP}. Standard errors were estimated via linear least-squares regression of Arrhenius plots. All energy values are in kcal mol^{-1}.

Compound	Solvent	E_a	ln$A$	$\Delta G^{\ddagger}$[a]	$\Delta\Delta H^{\ddagger}$[a][b]	$-\Delta(T\Delta S^{\ddagger})$ [a][b]	$\Delta\Delta G^{\ddagger}$[a,b]	k_{IP}/k_{BP}[a][c]	Ref.
1[i]	TCE[e]	26.4 ± 0.2	31.8 ± 0.3	25.0 ± 0.2[f]					[39]
4445⊙1[g]	TCE	24.5 ± 0.8	31.4 ± 1.2	23.3 ± 1.1[f]	1.9 ± 0.8[f]	–0.2 ± 0.8[f]	1.7 ± 1.1[f]	15/1[f]	[39]
3[i]	TCE[e]	29.8 ± 0.2	35.0 ± 0.2	26.1 ± 0.2[h]					[39]
4444Phe⊙3[g]	TCE	27.4 ± 0.3	30.6 ± 0.4	26.7 ± 0.4[h]	2.4 ± 0.3[h]	–3.0 ± 0.3[h]	–0.6 ± 0.4[h]	1/2.4[h]	[39]
2[i]	toluene[e]	28.7 ± 0.1	32.5 ± 0.1	26.6 ± 0.1					
4444Phe⊙2[i]	toluene[i]	25.9 ± 0.2	28.8 ± 0.3	26.5 ± 0.3	2.8 ± 0.2	–2.7 ± 0.2	0.1 ± 0.3	1.1/1	
4444Pen⊙2[i]	toluene[i]	26.5 ± 0.1	29.6 ± 0.2	26.5 ± 0.2	2.2 ± 0.1	–2.1 ± 0.1	0.1 ± 0.2	1.1/1	
444*o*X⊙2[i]	toluene[i]	26.3 ± 0.1	29.7 ± 0.2	26.3 ± 0.2	2.4 ± 0.1	–2.1 ± 0.1	0.3 ± 0.2	1.6/1	
4444S⊙2[g]	toluene	26.5 ± 0.3	29.2 ± 0.4	26.9 ± 0.4	2.1 ± 0.3	–2.4 ± 0.3	–0.3 ± 0.4	1/1.5	
4443⊙2[i]	toluene[i]	25.9 ± 0.2	29.1 ± 0.2	26.4 ± 0.2	2.7 ± 0.2	–2.5 ± 0.2	0.2 ± 0.2	1.4/1	
4442⊙2[i]	toluene[i]	26.1 ± 0.2	29.8 ± 0.3	26.0 ± 0.3	2.6 ± 0.2	–2.0 ± 0.2	0.6 ± 0.3	2.4/1	

[a] T = 359 K unless otherwise indicated. [b] $\Delta\Delta X^{\ddagger} = \Delta X^{\ddagger}$(free guest) – $\Delta X^{\ddagger}$(incarcerated guest). [c] k_{IP} = inner-phase rate constant; k_{BP} = bulk-phase rate constant. [d] Determined by UV/Vis spectroscopy. [e] Contained 5% CH_3COOH as carbene and aryldiazomethane trap. [f] T = 313 K. [g] Determined by ^{1}H NMR spectroscopy. [h] T = 345 K. [i] Contained 1% trifluoroacetic acid as aryldiazomethane trap.

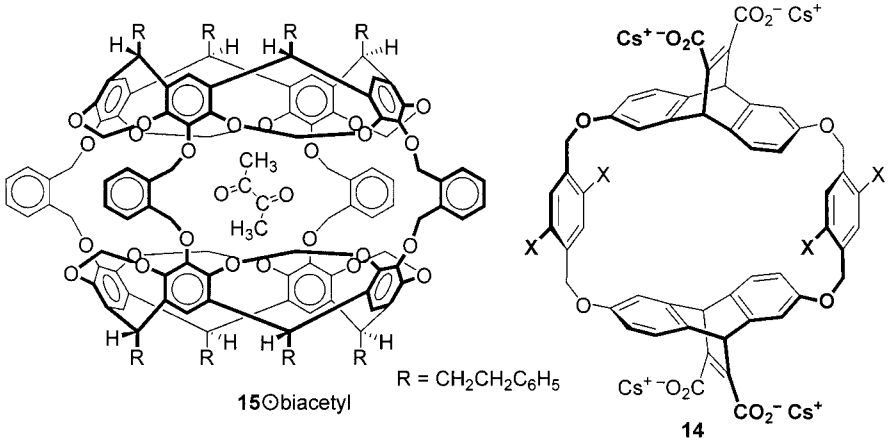

clophane host **14**, in which six electron-rich aromatic rings surround the transition state. Furthermore, the transition-state stabilization increased upon increasing the polarizability of the host's aryl units through substitution.

In the present study, the measured enthalpic transition-state stabilization is of similar magnitude. This suggests that also dispersion interactions are responsible for the enthalpic transition-state stabilization. Even though medium effects on the fragmentations of free diazirines are rarely observed,[40] we noted at least for **1**, which shows the largest rate change upon encapsulation, that solvent polarizability has the greatest influence on the thermal fragmentation rate constant. The rate constant k for the decomposition of **1** at 38.5 °C increases with increasing bulk-phase polarizability P and a plot of ln(k) against P shows a reasonable linear correlation (Figure 3). Minor contributions due to differences in cohesive pressure, polarity, viscosity and/or H-bond donor ability among the solvents might be responsible for the scattering of the data.[62,66]

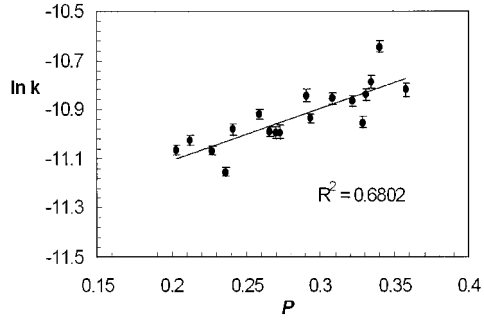

Figure 3. Dependence of the rate constant k for the thermolysis of **1** at 38.5 °C on the solvent polarizability $P = (n^2 - 1)/(n^2 + 2)$ (n = refractive index).

UV/Vis Spectroscopic Studies: The C–N bond breaking in all studied diazirines takes place in close vicinity to the four aryl units of a host's cavitand, which must provide an environment of very high polarizability and manifests itself

in bathochromic shifts of guest chromophores.[67] For example, Deshayes and co-workers observed large red shifts in the UV/Vis absorbance spectra of biacetyl hemicarceplexes.[20,21] Even though the origin of these red shifts is not fully clear, Marquez and Nau recently interpreted the red shifts with a predominant dependence of the n-π* transition energy of biacetyl on the polarizability *P* of the medium.[67] From a correlation between the exitation energy and solvent polarizability, they estimated a relative polarizability of *P* = 0.45 for the inner phase of hemicarcerand **15**, which is higher than the polarizabilities of common organic solvents. However, based on a more extended investigation, Deshayes, Piotrowiak and co-workers attribute the red shift to the decreased inner-phase free volume compared to the bulk solvent leading to a possible distortion of the biacetyl chromophore in the inner phase.[21]

In order to probe the inner-phase polarizability of the hemicarcerands used in this study, we applied a spectroscopic approach, which has been introduced recently by Nau and Marquez and which is based on solvochromic shifts of molecules with azo-chromophore.[67] During our kinetic UV/Vis spectroscopic experiments, we noticed large red shifts for the n-π* transition of the diazirine chromophore in the UV/Vis spectrum of all incarcerated aryldiazirines as compared to free diazirines in the bulk solvents. (Figure 4, Table 1, and Figure S3, S4 in supporting information). The small changes in λ_{max}, among the phenyldiazirine hemicarceplexes ($\Delta\lambda_{max}$ = 2.5 nm; Table 1 and Figure S4 in supporting information) likely reflect the small differences in the local environment around the diazirine chromophore inside each hemicarcerand.

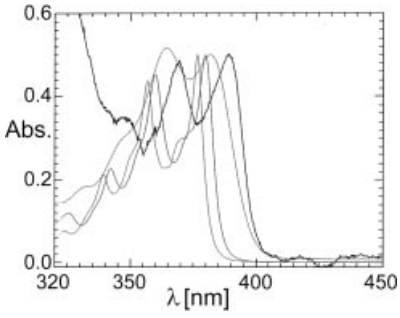

Figure 4. Normalized UV/Vis absorbance spectra of **1** in hexane (——), diphenyl ether (----) and perfluorohexane (-···-··) and of **4445⊙1** in tetrachloroethane (———).

We find a good linear correlation between the excitation energy of the lowest energy 0–0 transition of **1** and the solvent polarizability *P* as calculated according to the Clausius–Mosotti equation (Figure 5 and supporting information).[68] This suggests that λ_{max} of **1** depends mainly on the polarizability of the medium, similarly to biacetyl and 2,3-diazabicyclo[2.2.2]oct-2-ene.[67] Linear correlations between excitation energy and solvent polarizability *P* were also found for **2** and **3** (see Figure S1 and S2 in the supporting information) and allowed us to calculate the local inner-phase polarizability of the various hemicarcerands from the measured λ_{max} of the encapsulated diazirines (Table 1). Thus, the diazirines **1**–**3** can be used as reactants and polarizability probes to study the influence of the host on an encapsulated transition states. Polarizabilities range from 0.39 to 0.58. The inner-phase polarizability of the phenyldiazirine hemicarceplexes are remarkably close to the inner-phase polarizability of hemicarcerand **15** determined by Marquez and Nau.[67] Slightly higher polarizabilities are observed for **4445⊙1** and **4444⊙3**. This might reflect a better orientation of the diazirine chromophore with respect to the aryl units of the host leading to a stronger coupling of the transition dipole with the host's polarizability vector, or it might be a consequence of the low accuracy of this method for the determination of polarizability. Alternatively, the diazirine chromophore might be slightly distorted in some hemicarceplexes due to the different mix between occupied and empty space in the investigated hemicarceplexes leading to a shift in λ_{max}.[21] Further insight into the origin of the red shifts of encapsulated chromophores might be obtained from studies under pressure, which we are currently undertaking in our laboratory.

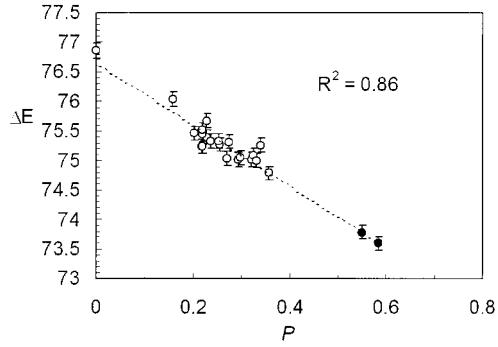

Figure 5. Plot of the excitation energy of the n-π* transition of **1** against the solvent polarizability function $P = (n^2 - 1)/(n^2 + 2)$ (*n* = refractive index) and best fit. The inner-phase polarizability of **4445** was determined from the best fit through extrapolation of the n-π* excitation energy for **4445⊙1** (black).

Inspection of the activation parameters in Table 2 shows that the enthalpic transition-state stabilization is partially or over-compensated by an unfavorable entropic contribution $\Delta T\Delta S^{\ddagger}$. In fact, all inner-phase transition states are entropically destabilized. We explain the unfavorable entropy term with the larger loss of vibrational degrees of freedom as the transition state is reached in the inner phase of the fairly rigid hemicarcerands as compared to the flexible and mobile solvent cage. A "tightening" of the hemicarceplexes along the reaction coordinate is expected based on ab initio calculations of the isomerization of phenyldiazirine to phenyldiazomethane (Figure 6).[69–72]

All stationary points shown in Figure 6 were optimized with the MP2 method using 6-31G basis sets. The energies were further improved through single point calculations using 6-311G+(d) basis sets. Transition states for the fragmentation of **2** to phenylcarbene and N_2 (TS1) and for the rebound of N_2 to yield diazomethane **13** (TS2) could be located, but not for the direct isomerization of **2** to **13**. However, it should be noted that Liu et al. were able to locate a transition state for the direct isomerization of di-

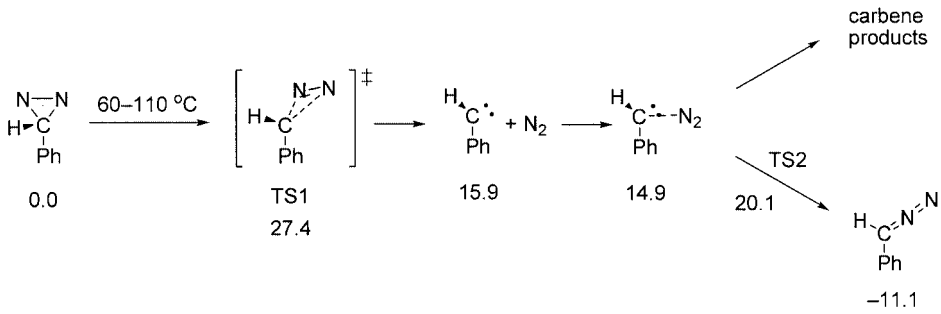

Figure 6. Mechanism of the thermal phenyldiazirine fragmentation and relative energies (E_o + ZPE in kcal/mol) of all stationary points and transition states at the MP2//6311G+(d)/6-31G level.

substituted diazirines to the corresponding diazomethanes (phenyl-*n*-butyldiazirine, 2-adamantane-2,3′-[3*H*]diazirine and phenylchlorodiazirine) by using the CASSCF method and 6-31G(d) basis sets.[48] The decomposition of **2** is endothermic by 15.9 kcal/mol with an computed activation energy of 27.4 kcal/mol in excellent agreement with the experimental E_a = 28.7 kcal/mol (Table 2). Optimized structures of **2** and TS1 are shown in Figure 7. In the transition state, the distance between the *para*-hydrogen and the most distal nitrogen increases from 6.329 Å to 6.419 Å, meaning that the guest slightly stretches upon reaching the transition state. Furthermore, both C–N bonds are considerably lengthened from 1.556 Å to 1.771 Å and 2.134 Å, respectively and the center of the dinitrogen moiety is rotated out of the phenyl plane. As a consequence, the transition state is stronger kinked as compared to the ground state.

Figure 7. Optimized structures (MP2//6-31G) of **2** (left) and TS1 (right); atom coloring: C, gray; N, black, H, white.

From the bend shape of the transition we would expect that $\Delta T\Delta S^{\ddagger}$ decreases if the hemicarcerand becomes more kinked such that its inner-phase shape closer resembles that of the transition state (Figure 7). We believe that this is the reason why the inner-phase phenyldiazirine decomposition rate constant increases with decreasing length of the linker X. In the order X = $(CH_2)_4$, (*S*,*S*)-$CH_2CH[OC(CH_3)_2O]CHCH_2$, $(CH_2)_3$, $(CH_2)_2$, *o*-$CH_2C_6H_4CH_2$ the tilt angle of the host α increases, whereas the center-to-center distance *d* between the host's cavitands decreases with increasing tilt. The measured activation parameters qualitatively support this analysis.

A plot of $\Delta\Delta G^{\ddagger}$, $\Delta T\Delta S^{\ddagger}$, and $\Delta\Delta H^{\ddagger}$ against α shows that $\Delta T\Delta S^{\ddagger}$ tends to decrease with increasing tilt of the inner phase and that the decrease of $\Delta\Delta G^{\ddagger}$ with increasing α has an entropic origin (Figure 8). This supports an induced-fit model. Even though the length of the inner phase decreases, the increased hemicarcerand bending leads to an improved fit between the inner phase and the bend transition state, which reduces the loss of vibrational degrees of freedom as the transition state is reached. Unfortunately, attempts to prepare phenyldiazirine hemicarceplexes **4445⊙2** and **444An⊙2**, in order to extend this correlation towards phenyldiazirine hemicarceplexes with larger tilt, failed.

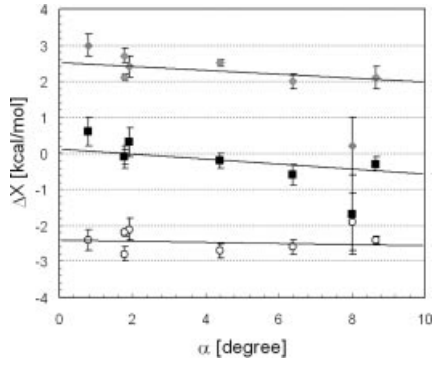

Figure 8. Dependence of $\Delta\Delta G^{\ddagger}$ (closed square), $\Delta T\Delta S^{\ddagger}$ (closed diamond), and $\Delta\Delta H^{\ddagger}$ (open circle) on the hemicarceplex tilt angle α. Data are taken from Table 1 and Table 2. Only the data from the phenyldiazirine hemicarceplexes have been used for the best fits.

The conclusions drawn from our investigation might be important for the design of hemicarcerand-based molecular reaction flasks in which high enantiomeric excesses in asymmetric reaction can be achieved. For example, the photochemical ring expansion of transient tolylcarbene in the inner phase of the nearly untilted hemicarcerand **4444S** led only to an enantiomeric excess of 7%.[11] We predict, that a

maximal enantiomeric excess in an asymmetric inner-phase reaction will result if the hemicarcerand is strongly twisted and also tilted. Such considerations should be especially important for example in asymmetric addition reactions to carbonyl compounds.

Experimental Section

General Remarks: All reactions were conducted under argon unless otherwise noted. HMPA was dried with activated molecular sieves (4 Å). Dichloromethane was dried with CaH_2 and distilled prior to use. Toluene, trifluoroacetic acid (TFA), tetrachloroethane (TCE) where purified by distillation. All other solvents were ACS grade or spectroscopic grade and were used as received. ^{1}H NMR and ^{13}C NMR spectra were recorded with a 200 MHz, 300 MHz or 400 MHz Varian FT NMR spectrometer. Spectra taken in $CDCl_3$, $CDCl_2CDCl_2$, CD_2Cl_2, or $C_6D_5CD_3$ were referenced to residual $CHCl_3$, $CHCl_2CDCl_2$, $CDHCl_2$ or $C_6D_5CD_2H$ at δ = 7.26, 5.99, 5.30 and 2.09 ppm, respectively. For VT-NMR studies, the temperature was calibrated using an ethylene glycol (>298 K) or methanol standard (< 298 K) and calibration curves that are implemented in the VNMR software. UV/Vis spectra were recorded with a Shimadzu UV-2401 Spectrophotometer. FT-IR spectra were recorded with a Nicolet FT-IR spectrophotometer equipped with a variable temperature cell holder and a magnetic cell stirrer. FAB-MS were obtained with a ZAB SE instrument with 3-nitrobenzyl alcohol matrix from the mass spectrometry laboratory at the University of Kansas, Lawrence, Kansas. HR-MALDI-TOF mass spectra were obtained with an Ion Spec HiResMALDI mass spectrometer. CHN elementary analysis were obtained from Desert Analytics, Tucson, Arizona. Gravity chromatography was performed on Bodman silica gel (70–230 mesh). Thin-layer chromatography involved aluminum-backed plates (silica gel 60, F_{254}, 0.25 mm).

Cyclobutabenzene-1(2*H*)-one oxime (**10**),[55] *tert*-butyl hypochlorite,[73] phenyldiazirine (**2**),[52,54] hemicarcerand **4445**,[51] diol host **4**,[51] and hemicarcecplexes **4444Phe⊙2**,[50] **4444Pen⊙2**,[15] **4444S⊙2**,[15] and **4444Phe⊙3**[39] were synthesized according to literature procedures.

Synthesis of *O*-Mesylcyclobutabenzene-1(2*H*)-one Oxime (11): Oxime **10** (1.5 g, 11.3 mmol) was dissolved in dry CH_2Cl_2 (60 mL) and cooled to 0 °C with stirring. Methanesulfonyl chloride (1 mL, 13 mmol) followed by triethylamine (1.73 mL, 12.4 mmol) were added and stirring was continued for one hour, after which the reaction was quenched with water (40 mL). The phases were separated. The aqueous layer was extracted with CH_2Cl_2 (3 × 10 mL). The combined organic layers were dried with $MgSO_4$ and concentrated under reduced pressure. The crude product (2.4 g) was flash-chromatographed (SiO_2; CH_2Cl_2) to yield **11** as a colorless solid (1.8 g, 77%). A small sample was recrystallized from hexanes. ^{1}H NMR (200 Hz, $CDCl_3$; 23°C) (2:1 mixture of isomers): δ = 7.55 (m, 2 H), 7.40 (m, 2 H), 4.06 (s, 2 H, minor isomer), 4.03 (s, 2 H, major isomer), 3.24 (s, 3 H) ppm. ^{13}C NMR (50.29 MHz, $CDCl_3$; 23°C): δ = 167.0 (minor), 159.2 (major), 145.9 (major), 145.0 (minor), 138.5 (minor), 137.7 (major), 134.7 (major), 134.2 (minor), 129.4 (major, minor) 124.7 (major), 123.9 (minor), 123.6 (major), 121.7 (minor), 40.6 (minor), 40.2 (major), 36.83 (minor), 36.78 (major) ppm. FT-IR (KBr) $\tilde{\nu}$ (cm^{-1}) = 3026.5 (m), 2939.8 (w), 1683.5 (m), 1585.2 (m), 1355.6 (s), 1180.4 (s), 974.0 (m), 814.1 (s), 759.6 (s), 637.9 (w), 521.2 (m) 431.6 (m). HR-FAB-MS (NBA-matrix): *m*/*z* = 212.0392 ([M + H]$^+$) (calcd. for $C_9H_{10}NSO_3$, 212.0381).

Synthesis of Spiro[cyclobutabenzene-1(2*H*),3′-diazirine] (12):[55] Compound **11** (2.3 g, 11 mmol) was dissolved in 51 mL dry ether. This solution was distributed equally over three 40-mL screw-cap vials. The solutions were cooled to –78 °C under Ar and were purged with dry ammonia gas until the volume in each vial had doubled. The vials were sealed with plastic screw caps containing Teflon liners and vigorously shaken for a few seconds after which they were placed in a precooled (–78 °C) steel reactor. The reactor was sealed and left at –25 °C for three days after which it was cooled to –78 °C and opened. The vials were removed and quickly opened (CAUTION, vials might be under pressure) and the content was poured into a 500-mL round-bottomed flask. After the reaction mixture had warmed to room temperature it was concentrated under reduced pressure. Due to the air sensitivity of **12**, the following steps were carried out under argon. The residue was suspended in argon-saturated water (40 mL) and extracted with argon-saturated CH_2Cl_2 (2 × 20 mL). The organic layers were washed with brine (20 mL), dried with $MgSO_4$ and concentrated to give crude **12** as a brownish solid. The crude product was dried for 30 min at high vacuum and was used for the next step without further purification. A small portion was recrystallized from ether/petroleum ether. ^{1}H NMR (400 MHz, $CDCl_3$; 23°C): δ = 7.36 (t, *J* = 7.6 Hz, 1 H), 7.29 (t, *J* = 7.6 Hz, 1 H), 7.24 (d, *J* = 7.6 Hz, 1 H), 7.08 (d, *J* = 7.2 Hz, 1 H), 3.76, 3.58 (AB-system, J_{AB} = 14.1 Hz, 2 H), 2.5 (m, 2 H, N*H*) ppm. ^{13}C NMR (100.56 MHz, $CDCl_3$; 23°C): δ = 145.2, 142.9, 130.5, 128.2, 122.9, 120.7, 63.7, 41.8 ppm. FAB-MS (NBA-matrix): *m*/*z* = 133.1 ([M + H]$^+$) (calcd. for $C_8H_9N_2$, 133.1).

Synthesis of Spiro[cyclobutabenzene-1(2*H*),3′-diazirine] (1):[55] Crude **12** from the previous step was dissolved in diethyl ether (80 mL) under argon and was cooled to 0 °C. A solution of *tert*-butyl hypochlorite (5 mL) in diethyl ether (7 mL) was added slowly in the dark over 15 minutes. After the reaction mixture had stirred for 1.5 hours at 0 °C, it was poured into ice-cold aqueous sodium metabisulfite (10%, 400 mL). The organic layer was separated and the aqueous layer extracted with petroleum ether (3 × 50 mL). The combined organic layers were washed with brine (30 mL), dried with $MgSO_4$ and concentrated at 0 °C. The residual crude oil was immediately purified by flash column chromatography (SiO_2; petroleum ether). The product fractions were concentrated at the rotavaporator until no petroleum ether was detectable by ^{1}H NMR to yield compound **1** as pail yellow oil (0.8 g, 56% yield over two steps). The product was stored in liquid nitrogen until it was further used. ^{1}H NMR (400 MHz, $CDCl_3$; 23°C): δ = 7.33 (t, *J* = 7.2 Hz, 1 H), 7.24 (t, *J* = 7.2 Hz, 1 H), 7.19 (d, *J* = 7.2 Hz, 1 H), 6.77 (d, *J* = 7.2 Hz, 1 H), 3.39, (s, 2 H) ppm. ^{13}C NMR (100.56 MHz, $CDCl_3$; 23°C): δ = 145.6, 142.9, 129.4, 128.3, 121.9, 119.8, 41.0, 37.0 ppm. UV/Vis (hexane): λ_{max} (ε) = 379.8 (430), 359.8 nm (390).

Synthesis of Hemicarceplex 4442⊙2 (Procedure A): A suspension of **4** (100 mg; 0.045 mmol), ethylene-1,2-diol ditosylate (**5**) (111 mg; 0.3 mmol), anhydrous cesium carbonate (0.9 g) and **2** (40 μL) in dry HMPA (5 mL) (***Caution:*** highly carcinogenic) was stirred under argon at room temperature in the dark for 5 days. The reaction mixture was poured into brine (20 mL) and filtered. The collected precipitate was washed with water (2 × 5 mL) and methanol (2 × 3 mL) and was dissolved in $CHCl_3$ (10 mL). After evaporation of the solvent, the residual crude product was dried under vacuum for 30 min. It was dissolved in the minimum amount of $CHCl_3$ and purified by preparative TLC (SiO_2; $CHCl_3$) to yield **4442⊙2** as a white powder (44 mg; 41% yield). ^{1}H NMR (200 MHz, CD_2Cl_2; 23°C): δ = 7.38–7.12 (m, 40 H, C_6H_5), 7.04 (s, 4 H, H_a), 6.97 (s, 2 H, H_a), 6.95 (s, 2 H, H_a), 5.76 (d, *J* = 6.8 Hz, 4 H, H_o), 5.79 [d, *J* = 7 Hz, 6 H, H_{ortho}(**2**), H_o], 5.19 [t, *J* = 7 Hz, 2 H, H_{meta}(**2**)], 4.82 (t, *J* = 7.4 Hz, 4 H, $CH_{methine}$), 4.81 (t, *J* = 7.4 Hz, 4 H, $CH_{methine}$), 4.3–4.16 (m, 12 H, OCH_2CH_2, H_i), 4.11 (d, *J* = 7.0 Hz, 4 H, H_i),

4.03 (br. s, 4 H, OCH_2CH$_2$), 3.38 [t, J = 7.1 Hz, 1 H, H$_{para}$(**2**)], 3.1 (br. s, 4 H, OCH_2CH_2O), 2.8–2.45 (m, 32 H, PhCH_2CH_2), 2.06 (br. s, 8 H, OCH$_2$CH_2), 2.06 (br. s, 8 H, OCH$_2$CH_2), 1.41 (m, 4 H, OCH$_2$CH_2), 0.27 [s, 1 H, CHN$_2$, (**2**)] ppm. ^{13}C NMR (50.29 MHz, CD_2Cl_2; 23°C): δ = 148.7, 148.6, 148.3, 147.3, 144.7, 144.4, 144.1, 142.3, 139.7, 139.4, 139.2, 139.0, 136.0 (**2**), 128.7, 128.7, 128.2 (**2**), 127.1 (**2**), 126.2, 123.5 (**2**), 115.1, 114.5, 113.4, 99.3, 99.0, 73.0, 72.8, 69.7, 37.4, 34.6, 32.9, 32.8, 28.4, 26.9, 21.3 (**2**) ppm. FAB-MS (NBA-matrix): m/z (%) = 2339.1 (71) [M + H]$^+$, 2311.5 (100) [M – N$_2$ + H]$^+$, 2221.7 (47) [M – **2** + H]$^+$. FT-IR ($CDCl_3$): $\tilde{\nu}$ (cm^{-1}) = 3081.5 (w), 3061.2 (w), 3028.2 (w), 2995.1 (w), 2944.3 (m), 2870.7 (m), 1602.9 (m), 1579.3 (w), 1497.0 (w), 1475.8 (s), 1466 (s), 1453.8 (m), 1441.2 (s), 1401.5 (w), 1373.2 (w), 1317.4 (s), 1156.8 (m), 1106.7 (m), 1066.9 (m), 1021.2 (s), 992.2 (s). UV/Vis (toluene): λ_{max} (ε) = 385.5 (550), 366.3 nm (630). $C_{149}H_{138}N_2O_{24}$ (2340.733): calcd. C 76.46, H 5.94, N 1.20; found C 76.52, H 5.55, N 1.25.

Synthesis of Hemicarceplex 4443⊙1: Application of procedure A to **4** (100 mg, 0.045 mmol) and propane-1,3-diol di-*p*-tosylate (**6**) (115 mg, 0.3 mmol) afforded hemicarceplex **4443⊙2** as a white powder in 32% yield. ^{1}H NMR (400 MHz, CD_2Cl_2; 23°C): δ = 7.30–7.12 (m, 40 H, C$_6H_5$), 6.98 (s, 4 H, H$_a$), 6.94 (s, 2 H, H$_a$), 6.92 (s, 2 H, H$_a$), 5.67 (d, J = 6.8 Hz, 4 H, H$_o$), 5.76–5.60 (m, 4 H, H$_o$), 5.62 [d, J = 7.6 Hz, 2 H, H$_{ortho}$(**2**)], 5.11 [t, J = 7.6 Hz, 2 H, H$_{meta}$(**2**)], 4.86 (t, J = 7.2 Hz, 4 H, CH$_{methine}$), 4.84 (t, J = 7.6 Hz, 4 H, CH$_{methine}$), 4.24–4.16 (m, 4 H, H$_i$), 4.18 (d, J = 7.2 Hz, 4 H, H$_i$), 4.06 (br. s, 8 H, OCH_2CH$_2$), 3.71 (s, broad, 8 H, OCH_2CH$_2$), 3.28 [t, J = 7.4 Hz, 1 H, H$_{para}$(**2**)], 2.78–2.62 (m, 16 H, PhCH_2CH$_2$), 2.54 (br. s, 16 H, PhCH$_2$CH_2), 2.06 (br. s, 10 H, OCH$_2$CH_2), 1.76 (br. s, 4 H, OCH$_2$CH_2), 0.17 [s, 1 H, CHN$_2$, (**2**)] ppm. ^{13}C NMR (50.29 MHz, CD_2Cl_2; 23°C): δ = 148.8, 148.6, 148.5, 144.9, 144.5, 142.0, 142.0, 139.5, 139.4, 138.9, 135.6 (**2**), 128.8, 128.7, 127.8 (**2**), 126.6 (**2**), 126.3, 123.4 (**2**), 114.9, 114.2, 98.6, 72.7, 37.5, 37.4, 34.9, 32.8, 32.0, 28.1, 27.7, 21.6 (**2**) ppm. FAB-MS (NBA-matrix): m/z (%) = 2353.2 (68) [M + H]$^+$, 2325.2 (100) [M – N$_2$ + H]$^+$, 2235.9 (57) [M – **2** + H]$^+$. FT-IR ($CDCl_3$): $\tilde{\nu}$ (cm^{-1}) = 3084.1 (w), 3061.2 (w), 3028.2 (w), 2992.6 (w), 2949.4 (m), 2875.7 (m), 1603.7 (w), 1580.3 (w), 1496.9 (w), 1475.9 (s), 1467.1 (s), 1453.7 (m), 1442.6 (s), 1399.8 (w), 1374.4 (w), 1317.2 (s), 1155.9 (s), 1106.7 (m), 1067.8 (m), 1020.7 (s), 991.5 (s). UV/Vis (toluene): λ_{max} (ε) = 387.2 (660), 367.5 (760). $C_{150}H_{140}N_2O_{24}$ (2354.76): calcd. C 76.51, H 5.99, N 1.19; found C 76.58, H 5.84, N 1.21.

Synthesis of Hemicarceplex 444*o*X⊙2: Application of procedure A to **4** (100 mg, 0.045 mmol) and α,α-dibromo-*o*-xylene (**7**) (48 mg, 0.182 mmol) afforded hemicarceplex **444*o*X⊙2** as a white powder in 45% yield. ^{1}H NMR (400 MHz, $CDCl_3$; 23°C): δ = 7.32 (s, 4 H, CH$_2$C$_6H_4$CH$_2$), 7.30–7.12 (m, 40 H, C$_6H_5$), 6.97 (s, 6 H, H$_a$), 6.93 (s, 2 H, H$_a$), 6.92 (s, 2 H, H$_a$), 5.67 (br. s, 4 H, H$_o$), 5.55 [d, J = 7.2 Hz, 2 H, H$_{ortho}$(**2**)], 5.50 (m, J = 7.2 Hz, 4 H, H$_o$), 5.03 [t, J = 7.6 Hz, 2 H, H$_{meta}$(**2**)], 4.84 (t, J = 7.6 Hz, 4 H, CH$_{methine}$), 4.83 (t, J = 7.6 Hz, 4 H, CH$_{methine}$), 4.9–4.7 (m, 4 H, CH_2C$_6$H$_4$CH_2) 4.16 (d, J = 6.4 Hz, 4 H, H$_i$), 4.07 (d, J = 7.2 Hz, 4 H, H$_i$), 4.23–3.3 (several broad multiplets, 12 H, OCH_2CH$_2$), 3.16 [t, J = 7.2 Hz, 1 H, H$_{para}$(**2**)], 2.78–2.62 (m, 16 H, PhCH_2CH$_2$), 2.60–2.43 (m, 16 H, PhCH$_2$CH_2), 2.00 (s, 8 H, OCH$_2$CH_2), 1.72 (s, 4 H, OCH$_2$CH_2), 0.11 [s, 1 H, CHN$_2$, (**2**)] ppm. ^{13}C NMR (50.29 MHz, CD_2Cl_2; 23°C): δ = 148.9, 148.8, 145.4, 144.8, 144.6, 142.1, 139.3, 139.0, 138.5, 136.5, 135.5 (**2**), 130.2, 128.8, 128.7, 128.5, 127.8 (**2**), 126.4 (**2**), 126.3, 123.4 (**2**), 114.8, 114.2, 98.7, 74.3, 72.9, 72.5, 37.5, 34.9, 32.9, 32.8, 27.9, 27.6, 21.6 (**2**) ppm. FAB-MS (NBA-matrix): m/z (%) = 2414.1 (58) [M + H]$^+$, 2387.0 (46) [M – N$_2$ + H]$^+$, 2298.1 (100) [M – **2** + H]$^+$. FT-IR ($CDCl_3$): $\tilde{\nu}$ (cm^{-1}) = 3086.6 (w), 3063.7 (w), 3025.6 (w), 2995.1 (w), 2946.9 (m), 2873.2 (m), 1603.3 (w), 1578.9 (w), 1496.8 (w), 1475.8 (s), 1467.3 (s), 1453.8 (m), 1441.4 (s), 1399.6 (w), 1373.8 (w), 1316.6 (s), 1155.5 (m), 1105.9 (m), 1082.6 (m), 1019.9 (s), 991.1 (s). UV/Vis (toluene): λ_{max} (ε) = 387.1 (520), 367.3 (670). $C_{155}H_{142}N_2O_{24}$ (2416.831): calcd. C 77.03, H 5.92, N 1.16; found C 76.96, H 6.08, N 1.25.

In situ Preparation of Hemicarceplex 4445⊙1: Hemicarcerand **4445** (45.5 mg, 0.02 mmol) was dried overnight at 120 °C under high vacuum (<0.01 mm) and was dissolved in $CDCl_2CDCl_2$ (0.5 mL). The solution was cooled to 0 °C before neat **1** (105 μL) was added. The clear solution was kept in the dark at 0 °C. After 50 minutes a sample (40 μL) was taken via syringe and diluted with $CDCl_2CDCl_2$ (0.45 mL) in a NMR tube. The ^{1}H NMR spectrum, taken immediately, showed approximately 85% hemicarceplex **4445⊙1** formation. The product hemicarceplex was precipitated by the addition of precooled methanol (5 mL, –30 °C). The precipitate was rapidly collected on a glass sinter, washed with cold methanol (2 × 1 mL; –15 °C), transferred into a 5-mL round-bottomed flask and dried under high vacuum (< 0.01 mm) at –10 to –12 °C for 30 minutes. Crude **4445⊙1** (39 mg, 80% purity) was stored in liquid N$_2$ and was used for the thermolysis studies without further purification. ^{1}H NMR (400 MHz; $C_6D_5CD_3$; –10 °C): δ = 7.20–7.00 (m, 40 H, C$_6H_5$), 6.96 (s, 6 H, H$_a$), 6.89 (t, J = 7.6 Hz, 1 H, H$_{aryl}$ (**1**)), 6.36 (d, J = 7.6 Hz, 1 H, H$_{aryl}$ (**1**)), 5.74–5.64 (m, 8 H, H$_o$), 5.07–4.99 (m, 8 H, CH$_{methine}$) 4.26 (d, J = 7.6 Hz, 4 H, H$_i$), 4.23 (d, J = 6.8 Hz, 4 H, H$_i$), 4.08–3.66 (several broad multiplets, 16 H, OCH_2CH$_2$), 3.62 [d, J = 7.6 Hz, 1 H, H$_{aryl}$ (**1**)], 3.43 [t, J = 7.4 Hz, 1 H, H$_{aryl}$ (**1**)], 2.73 [s, 2 H, CH$_2$ (**1**)], 2.64–2.53 (m, 16 H, PhCH_2CH$_2$), 2.52–2.37 (m, 16 H, PhCH$_2$CH_2), 1.9–1.56 [m, 18 H, OCH$_2$CH_2, OCH$_2$(CH_2)$_3$CH$_2$O] ppm. FAB-MS (NBA-matrix): m/z (%) = 2392.9 (52) [M + H]$^+$, 2363.8 (65) [M – N$_2$ + H]$^+$, 2263.3 (100) [M – **1** + H]$^+$. UV/Vis (toluene) λ_{max} (ε) = 389.1 (530), 369.3 (515).

Thermolysis Studies. (a) ^{1}H NMR Experiments (Method A): A solution of hemicarceplex **4444Pen⊙2**, **4444Phe⊙3**, **4444S⊙2** or **4445⊙1** (4–7 mg) was dissolved in 550 μL $CDCl_2CDCl_2$ or $C_6D_5CD_3$ and was placed in a NMR tube, which was sealed with a Teflon screw cap. For the thermolysis of hemicarceplex **4445⊙1**, the NMR tube was inserted into the temperature-equilibrated probe of the 400 MHz NMR spectrometer. After further temperature equilibration (approx. 10 minutes), ^{1}H NMR spectra were recorded periodically until all **4445⊙1** had decomposed. Rate constants were determined from the time-dependent intensity change of the doublet at δ = 6.36 ppm, which is assigned to an aryl proton of encapsulated **1**. For the thermolysis of hemicarceplexes **4444Pen⊙2**, **4444Phe⊙3**, and **4444S⊙2**, the sample was heated in a constant temperature bath for a given time and rapidly cooled by immersing it into ice/water. The progress of the thermolysis was followed by ^{1}H NMR spectroscopy at room temperature. Typically, 10–15 ^{1}H NMR spectra were recorded in each experiment. The relative amount of unreacted hemicarceplex was determined from the integral of selected guest protons relative to the integral of the methylene protons of the phenethyl feet groups of host **4444Phe**, or the methyl protons of the pentyl groups of host **4444S** and **4444Pen**: **4444Pen⊙2**: s at δ = 0.11 [H$_{diazirine}$(**2**)]; **4444Phe⊙3**: s at δ = –1.90 ppm [CH_3(**3**)]; **4444S⊙2**: s at δ = 0.24 [H$_{diazirine}$(**2**)].

(b) UV/Vis Spectroscopic Experiments. (Method B): Kinetic UV/Vis experiments were carried out with a Shimadzu UV/Vis spectrophotometer equipped with a variable-temperature cuvette holder and magnetic cuvette stirrer. The cuvette holder was heated with a circulating iso-temperature bath. In a typical experiment, a solution of hemicarceplex in toluene/trifluoroacetic acid, 99:1 (v/v) was placed in a 1 × 1 cm quartz cuvette containing a stirring bar. The cuvette was closed with a Teflon stopper, inserted into the pre-

heated cuvette holder and equilibrated for approximately 15 minutes. Control experiments, in which a Teflon-coated thermocouple was immersed into the reaction solution, showed that after this time the solution in the cuvette was fully temperature-equilibrated. The absorbance at λ = 387 nm and 367 nm was recorded as function of time in the kinetic mode of the instrument. The concentration of the solution was adjusted such that the initial absorbance was around 0.05–0.10. Typically 2000 to 3000 data points were collected per run and were fitted to a mono-exponential decay. The experimental temperature was determined using a calibrated thermocouple, which was immersed into the hot reaction solution after the kinetic run. Control experiments showed that both methods (UV/Vis and ^{1}H NMR) gave identical rate constants within the accuracy of each method.

Content of the Supporting Information: Tables with rate constants for the decomposition of **4444Pen⊙2**, **4444Phe⊙2**, **4444S⊙2**, **4442⊙2**, **4443⊙2**, and **444*o*X⊙2**, and **2**. Tables with λ_{max} in different solvents for **1**–**3**. Correlations between excitation energy and solvent polarizability for **2** and **3**. Table with hemicarcerand induced upfield shift of the guest protons inside **4444Pen⊙2**, **4444Phe⊙2**, **4444S⊙2**, **4442⊙2**, **4443⊙2**, and **444*o*X⊙2**. Table with rate constants for the thermal decomposition of **1** in different solvents. Partial UV/Vis spectra of **2** in different solvents and of **4444Pen⊙2**, **4444Phe⊙2**, **4444S⊙2**, **4442⊙2**, **4443⊙2**, and **444*o*X⊙2** in toluene. Energy and optimized geometry of all stationary points shown in Figure 6.

Acknowledgments

The authors warmly thank the National Science Foundation (Grant CHE-0075749) for generous financial support of this project.

[1] D. J. Cram, J. M. Cram, *Container Molecules and Their Guests* (Ed.: J. F. Stoddart), The Royal Society of Chemistry, Cambridge, U. K. **1994**, 131–216.
[2] A. Jasat, J. C. Sherman, *Chem. Rev.* **1999**, *99*, 931–967.
[3] R. Warmuth, J. Yoon, *Acc. Chem. Res.* **2001**, *34*, 95–105.
[4] M. M. Conn, J. Rebek, Jr., *Chem. Rev.* **1997**, *97*, 1647–1668.
[5] J. de Mendoza, *Chem. Eur. J.* **1998**, *4*, 1373–1377.
[6] R. Warmuth, *J. Inclusion Phenom.* **2000**, *37*, 1–38.
[7] J.-P. Bourgeois, M. Fujita, *Aust. J. Chem.* **2002**, *55*, 619–621.
[8] D. J. Cram, M. E. Tanner, R. Thomas, *Angew. Chem.* **1991**, *103*, 1048–1051; *Angew. Chem. Int. Ed. Engl.* **1991**, *30*, 1024–1027.
[9] R. Warmuth, *Angew. Chem.* **1997**,*109*, 1406–1409; *Angew. Chem. Int. Ed. Engl.* **1997**, *36*, 1347–1350.
[10] R. Warmuth, *Chem. Commun.* **1998**, 59–60.
[11] R. Warmuth, *J. Am. Chem. Soc.* **2001**, *123*, 6955–6956.
[12] J.-L. Kerdelhué, R. Warmuth, K. J. Langenwalter, *J. Am. Chem. Soc.* **2003**, *125*, 973–986.
[13] D. A. Makeiff, K. Vishnumurthy, J. C. Sherman, *J. Am. Chem. Soc.* **2003**, *125*, 9558–9559.
[14] P. Roach, R. Warmuth, *Angew. Chem.* **2003**, *115*, 3147–3150; *Angew. Chem. Int. Ed.* **2003**, *42*, 3039–3042.
[15] R. Warmuth, M. A. Marvel, *Chem. Eur. J.* **2001**, *7*, 1209–1220.
[16] M. Ziegler, J. L. Brumaghim, K. N. Raymond, *Angew. Chem.* **2000**, *112*, 4285–4287; *Angew. Chem. Int. Ed.* **2000**, *39*, 4119–4121.
[17] a) M. Yoshizawa, T. Kusukawa, M. Fujita, S. Sakamoto, K. Yamaguchi, *J. Am. Chem. Soc.* **2001**, *123*, 10454–10459.
[18] A. Farran, K. D. Deshayes, C. Matthews, I. Balanescu, *J. Am. Chem. Soc.* **1995**, *117*. 9614–9615.
[19] Z. S. Romanova, K. Deshayes, P. Piotrowiak, *J. Am. Chem. Soc.* **2001**, *123*, 2444–2445.
[20] A. Farran, K. D. Deshayes, *J. Phys. Chem.* **1996**, *100*, 3305–3307.
[21] Z. S. Romanova, K. Deshayes, P. Piotrowiak, *J. Am. Chem. Soc.* **2001**, *123*, 11029–11036.
[22] S. Mendoza, P. D. Davidov, A. E. Kaifer, *Chem. Eur. J.* **1998**, *4*, 864–870.
[23] S. K. Kurdistani, R. C. Helgeson, D. J. Cram, *J. Am. Chem. Soc.* **1995**, *117*, 1659–1660.
[24] T. A. Robbins, D. J. Cram, *J. Am. Chem. Soc.* **1993**, *115*, 12199.
[25] R. Warmuth, E. F. Maverick, C. B. Knobler, D. J. Cram, *J. Org. Chem.* **2003**, *68*, 2077–2088.
[26] J. Kang, J. Rebek Jr., *Nature* **1996**, *385*, 50–52.
[27] J. Kang, J. Santamaría, G. Hilmersson, J. Rebek Jr., *J. Am. Chem. Soc.* **1998**, *120*, 7389–7390.
[28] T. Kusukawa, T. Nakai, T. Okano, M. Fujita, *Chem. Lett.* **2003**, *32*, 284–5.
[29] M. Yoshizawa, Y. Takeyama, T. Kusukawa, M. Fujita, *Angew. Chem.* **2002**, *114*, 1403–1405; *Angew. Chem. Int. Ed.* **2002**, *41*, 1347–1349.
[30] M. Yoshizawa, Y. Takeyama, T. Okano, M. Fujita, *J. Am. Chem. Soc.* **2003**, *125*, 3243–3247.
[31] S. K. Körner, F. C. Tucci, D. M. Rudkevich, T. Heinz, J. Rebek Jr., *Chem. Eur. J.* **2000**, *6*, 187–195.
[32] J. Rebek, Jr., J. Chen, *Org. Lett.* **2002**, *4*, 327–329.
[33] A. M. A. van Wageningen, P. Timmerman, J. P. M. van Duynhoven, W. Verboom, F. C. J. M. van Veggel, D. N. Reinhoudt, *Chem. Eur. J.* **1997**, *3*, 639–654.
[34] J. Chen, S. Körner, S. L. Craig, S. Lin, D. M. Rudkevich, J. Rebek, Jr., *PNAS* **2002**, *99*, 2593–2596.
[35] K. Kumazawa, K. Biradha, T. Kusukawa, T. Okano, M. Fujita, *Angew. Chem.* **2003**, *115*, 4039–4043; *Angew. Chem. Int. Ed.* **2003**, *42*, 3909–3913.
[36] R. Wolfenden, M. Snider, C. Ridgway, B. Miller, *J. Am. Chem. Soc.* **1999**, *121*, 7419–7420.
[37] A. Warshel, *J. Biol. Chem.* **1998**, *273*, 27035–27038.
[38] W. R. Cannon, S. J. Benkovic, *J. Biol. Chem.* **1998**, *273*, 26257–26260.
[39] R. Warmuth, J.-L. Kerdelhué, S. Sánchez Carrera, K. J. Langenwalter, N. Brown, *Angew. Chem.* **2002**, *114*, 102–105; *Angew. Chem. Int. Ed.* **2002**, *41*, 96–99.
[40] M. T. H. Liu, *Chem. Soc. Rev.* **1982**, *11*, 127–140.
[41] M. T. H. Liu, M. Tencer, I. D. R. Stevens, *J. Chem. Soc. Perkin Trans. 2* **1986**, 211–214.
[42] I. D. R. Stevens, M. T. H. Liu, N. Soundararajan, N. Paike, *J. Chem. Soc. Perkin Trans. 2* **1990**, 661–667.
[43] M. T. H. Liu, I. Yamamoto, *Can. J. Chem.* **1979**, *57*, 1299–1303.
[44] D. J. Cram, M. T. Blanda, K. Paek, C. B. Knobler, *J. Am. Chem. Soc.* **1992**, *114* 7165–1113.
[45] A. E. Keating, M. A. Garcia-Garibay, K. N. Houk, *J. Am. Chem. Soc.* **1997**, *119*, 10805–10809.
[46] D. M. Miller, P. R. Schreiner, H. F. Schaefer, III, *J. Am. Chem. Soc.* **1995**, *117*, 4137–4143.
[47] B. Bigot, R. Ponec, A. Sevin, A. Devaquet, *J. Am. Chem. Soc.* **1978**, *100*, 6575–6580.
[48] M. T. H. Liu, Y.-K. Choe, M. Kimura, K. Kobayashi, S. Nagase, T. Wakahara, Y. Niino, M. O. Ishitsuka, Y. Maeda, T. Akasaka, *J. Org. Chem.* **2003**, *68*, 7471–7478.
[49] B. M. Jennings, M. T. H. Liu, *J. Am. Chem. Soc.* **1976**, *98*, 6416–6417.
[50] C. Kemmis, R. Warmuth, *Supramol. Chem.* **2003**, 253–267.
[51] J. Yoon, C. Sheu, K. N. Houk, C. B. Knobler, D. J. Cram, *J. Org. Chem.* **1996**, *61*, 9323–9339.
[52] E. Schmitz, *Chem. Ber.* **1962**, *95*, 688–691.
[53] R. A. G. Smith, J. R. Knowles, *J. Chem. Soc. Perkin Trans. 1I* **1975**, 686–699.
[54] The crude ^{1}H NMR spectrum of thermally decomposed **4445⊙1** shows four AB systems between δ = –0.4 to –0.6 ppm, consistent with the expected number of isomeric carbene-host

reaction products resulting from addition of **1** to a cavitands aryl unit.
[55] K. M. Broadus, S. R. Kass, *J. Org. Chem.* **2000**, *65*, 6566–6571.
[56] J. M. Goodman, W. C. Still, *J. Comput. Chem.* **1991**, *12*, 1110–1117.
[57] N. L. Allinger, *J. Am. Chem. Soc.* **1977**, *99*, 8127–8134.
[58] W. C. Still, A. Tempczyk, R. C. Hawley, T. Hendrickson, *J. Am. Chem. Soc.* **1990**, *112*, 6127–6129.
[59] C. Sheu, K. N. Houk, *J. Am. Chem. Soc.* **1996**, *118*, 8056–8070.
[60] In fact D. J. Cram and co-workers came to very similar conclusions for **4442**, **4443** based on CPK model studies see ref.[51].
[61] M. J. Dewar, L. E. Wade, Jr., *J. Am. Chem. Soc.* **1977**, *99*, 4417–4424.
[62] A. R. Firestone, M. A. Vitale, *J. Org. Chem.* **1981**, *46*, 2160–2164.
[63] A. McCurdy, L. Jimenez, D. A. Stauffer, D. A. Dougherty, *J. Am. Chem. Soc.* **1992**, *114*, 10314–10321.
[64] D. A. Stauffer, R. E. Barrans, Jr., D. A. Dougherty, *Angew. Chem.* **1990**, *102*, 953–956; *Angew. Chem. Int. Ed. Engl.* **1990**, *29*, 915–918.
[65] S. M. Ngola, D. A. Dougherty, *J. Org. Chem.* **1996**, *61*, 4355–4360.
[66] C. Reichardt, *Solvents and Solvent Effects in Organic Chemistry*, 2nd ed. Wiley-VCH, Weinheim, **1988**.
[67] C. Marquez, W. M. Nau, *Angew. Chem.* **2001**, *113*, 4515–4518; *Angew. Chem. Int. Ed. Engl.* **2001**, *40*, 4387–4390.
[68] a) P. Suppan, N. Ghoneim, *Solvatochromism*, The Royal Society of Chemistry, Cambridge, **1997**.
[69] A. D. Becke, *Phys. Rev. A* **1988**, *38*, 3098–3100.
[70] C. Lee, W. Yang, R. G. Parr, *Phys. Rev. B* **1988**, *37*, 785–789.
[71] A. D. Becke, *J. Chem. Phys.* **1993**, *98*, 5648–5652.
[72] Gaussian 03, Revision B.02, Gaussian, Inc., M. J. Frisch, G. W. Trucks, H. B. Schlegel, G. E. Scuseria, M. A. Robb, J. R. Cheeseman, J. A. Montgomery, Jr., T. Vreven, K. N. Kudin, J. C. Burant, J. M. Millam, S. S. Iyengar, J. Tomasi, V. Barone, B. Mennucci, M. Cossi, G. Scalmani, N. Rega, G. A. Petersson, H. Nakatsuji, M. Hada, M. Ehara, K. Toyota, R. Fukuda, J. Hasegawa, M. Ishida, T. Nakajima, Y. Honda, O. Kitao, H. Nakai, M. Klene, X. Li, J. E. Knox, H. P. Hratchian, J. B. Cross, C. Adamo, J. Jaramillo, R. Gomperts, R. E. Stratmann, O. Yazyev, A. J. Austin, R. Cammi, C. Pomelli, J. W. Ochterski, P. Y. Ayala, K. Morokuma, G. A. Voth, P. Salvador, J. J. Dannenberg, V. G. Zakrzewski, S. Dapprich, A. D. Daniels, M. C. Strain, O. Farkas, D. K. Malick, A. D. Rabuck, K. Raghavachari, J. B.Foresman, J. V. Ortiz, Q. Cui, A. G. Baboul, S. Clifford, J. Cioslowski, B. B. Stefanov, G. Liu, A. Liashenko, P. Piskorz, I. Komaromi, R. L. Martin, D. J. Fox, T. Keith, M. A. Al-Laham, C. Y. Peng, A. Nanayakkara, M. Challacombe, P. M. W. Gill, B. Johnson, W. Chen, M. W. Wong, C. Gonzalez, J. A. Pople, Pittsburgh PA, **2003**.
[73] M. J. Mintz, C. Walling, *Org. Synth. Coll.* **1963**, *4*, 184–185.

Received: August 13, 2004

